Quantitative XANES Spectroscopy Study on the Prototype Hole- and Electron-Doped High-T_c Superconductor Systems, $(La,Sr)_2CuO_4$ and $(Nd,Ce)_2CuO_4$

Y. Tanaka,[†] M. Karppinen,*[,†,‡] T. Kobayashi,[†] T. S. Chan,[§] R. S. Liu,[§] J. M. Chen,[||] and H. Yamauchi[†,‡]

Materials and Structures Laboratory, Tokyo Institute of Technology, Yokohama 226-8503, Japan, Laboratory of Inorganic Chemistry, Department of Chemistry, Helsinki University of Technology, FI-02015 TKK, Finland, Department of Chemistry, National Taiwan University, Taipei 106, Taiwan, Republic of China, and National Synchrotron Radiation Research Center, Hsinchu 30076, Taiwan, Republic of China

Received March 28, 2008. Revised Manuscript Received May 31, 2008

Here we demonstrate that the Cu L-edge XANES (X-ray absorption near-edge structure) spectroscopy can be employed for quantitative analysis of the level of carrier-doping in the prototype hole- and electron-doped high-T_c superconductor systems, $(La_{1-x}Sr_x)_2CuO_{4+\delta}$ and $(Nd_{1-x}Ce_x)_2CuO_{4+\delta}$. The progress in hole-doping in the $(La_{1-x}Sr_x)_2CuO_{4+\delta}$ system is seen as development of the shoulder peak (due to nominally trivalent copper) on the high-energy side of the main peak (due to nominally divalent copper) in the Cu L_3-edge region, whereas the progress in electron-doping in the $(Nd_{1-x}Ce_x)_2CuO_{4+\delta}$ system results in an additional absorption peak at about 934 eV (due to nominally monovalent copper), together with a decrease in the intensity of the main peak (due to nominally divalent copper). On the basis of these features, Cu-valence values are quantitatively obtained in excellent agreement with those calculated for the same samples from the precise oxygen contents, $4+\delta$, determined by means of wet-chemical analysis. The valence of Ce in $(Nd_{1-x}Ce_x)_2CuO_{4+\delta}$ is revealed to be somewhat lower than +4 (ca. +3.8) on the basis of Ce M_5-edge XANES data. In the O K-edge XANES spectra, the increase in the CuO_2-plane hole concentration with increasing x in $(La_{1-x}Sr_x)_2CuO_{4+\delta}$ is seen as an enhancement in the intensity of the pre-edge feature at ~528.9 eV, whereas for $(Nd_{1-x}Ce_x)_2CuO_{4+\delta}$, no signs are observed that could be directly assigned to the change in electron-doping level.

Introduction

In layered copper oxides, high-T_c superconductivity occurs upon doping the constituent CuO_2 planes with either holes (*p*-type doping) or electrons (*n*-type doping). The simplest *p*-type copper-oxide superconductor, $(La_{1-x}Sr_x)_2CuO_{4+\delta}$, is composed of a one-by-one stacking of a rock-salt-structured (La,Sr)O−(La,Sr)O block and a single CuO_2 plane (so-called *T*-structure), whereas the analogous *n*-type copper-oxide superconductor, $(Nd_{1-}Ce_x)_2CuO_{4+\delta}$, possesses a so-called *T′*-structure in which a fluorite-structured (Nd,Ce)−O_2−(Nd,Ce) block alternates with an apical-oxygen-free CuO_2 plane. The $(La_{1-x}Sr_x)_2CuO_{4+\delta}$ phase shows superconductivity once the CuO_2 plane is doped with a proper amount of holes through either excess oxygen doping or aliovalent Sr^{II}-for-La^{III} cation substitution. On the other hand, occurrence of superconductivity in $(Nd_{1-x}Ce_x)_2CuO_{4+\delta}$ requires not only that the proper amount of electrons is doped through Ce^{IV}-for-Nd^{III} substitution but also that the properly doped sample is postannealed under a low oxygen partial pressure;[1] the main role of the low-oxygen-partial-pressure annealing is most likely to repair the Cu vacancies apparently present in small concentrations in as-air-synthesized $(Nd_{1-x}Ce_x)_2CuO_{4+\delta}$ samples.[2,3] Another difference between the two systems is that for $(Nd_{1-x}Ce_x)_2CuO_{4+\delta}$ superconductivity seems to appear in a much narrower doping range ($0.07 \leq x \leq 0.09$) than for $(La_{1-x}Sr_x)_2CuO_{4+\delta}$ ($0.03 \leq x \leq 0.125$).

Various spectroscopic techniques have been employed to get insights into the electronic structures of both the *p*- and *n*-type copper oxides. X-ray absorption near-edge structure (XANES) spectroscopy at O K, Cu K, and Cu $L_{2,3}$ absorption edges in particular provides us with tools to probe in a site-selective manner the local densities of unoccupied O 2p and Cu 3d states near the Fermi level. The parent La_2CuO_4 and Nd_2CuO_4 compounds are believed to be charge-transfer insulators in which the *p*-type doping introduces holes in the valence band of predominantly O 2p character and the *n*-type doping introduces electrons in the conduction band (upper Hubbard band, UHB) of predominantly Cu 3d character. Formation of O 2p holes in the valence band is readily observed as a development of additional absorption peaks in both O K-edge and Cu $L_{2,3}$-edge (due to strong Cu

* Corresponding author. E-mail: maarit.karppinen@tkk.fi.
[†] Tokyo Institute of Technology.
[‡] Helsinki University of Technology.
[§] National Taiwan University.
[||] National Synchrotron Radiation Research Center.

(1) Takagi, H.; Uchida, S.; Tokura, Y. *Phys. Rev. Lett.* **1989**, *62*, 1197.
(2) Kang, H. J.; Dai, P.; Campbell, B. J.; Chupas, P. J.; Rosenkranz, S.; Lee, P. L.; Huang, Q.; Li, S.; Komiya, S.; Ando, Y. *Nat. Mater.* **2007**, *6*, 224.
(3) Tanaka, Y.; Motohashi, T.; Karppinen, M.; Yamauchi, H. *J. Solid State Chem.* **2008**, *181*, 365.

10.1021/cm800892z CCC: $40.75
Published on Web 07/26/2008

3d−O 2p hybridization) XANES spectra. These features have been successfully utilized for quantitative analyses of the doping level in various hole-doped copper-oxide systems such as $CuBa_2RCu_2O_{7-\delta}$,[4,5] $Tl_2Ba_2CaCu_2O_{8+\delta}$,[6] $Bi_2Sr_2Ca_{n-1}Cu_nO_{4+2n+\delta}$ ($n = 2, 3$),[7–11] $HgBa_2Ca_{n-1}Cu_nO_{3+2n-\delta}$ ($n = 1, 2, 3$),[12–14] $(Pb_{2/3}Cu_{1/3})_3Ba_2YCu_2O_{8+\delta}$,[15] $CuBa_2Ca_2Cu_3O_{9-\delta}$,[16] and $Cu(Sr,Ba)_2(R,Ce)_sCu_2O_{5+2s+\delta}$,[17] but not yet for the simplest *p*-type system $(La_{1-x}Sr_x)_2CuO_{4+\delta}$. As for the *n*-type doping, previous XANES studies on the $(Nd_{1-x}Ce_x)_2CuO_{4+\delta}$ system have revealed that the electrons introduced upon the Ce^{IV}-for-Nd^{III} substitution fill the hole states with 3d character at the Cu site[18–24] to form Cu^+ species.[22–25] Accordingly, reduction in the intensity of the peak due to empty Cu 3d states (i.e., formally divalent copper) in the Cu $L_{2,3}$-edge spectrum has been considered as the most visible signature of the *n*-type doping.[18–21] However, no quantitative XANES studies in regards to the doping level have been reported for $(Nd_{1-x}Ce_x)_2CuO_{4+\delta}$.

Here we present quantitative Cu $L_{2,3}$-edge and O K-edge XANES results for the prototype *p*- and *n*-type high-T_c superconductor systems, $(La_{1-x}Sr_x)_2CuO_{4+\delta}$ and $(Nd_{1-x}Ce_x)_2CuO_{4+\delta}$, using in both cases series of samples with systematically varied carrier-doping levels. The XANES results show nearly perfect agreement with the hole or electron concentrations calculated for the same samples from the precise oxygen-content parameter δ as determined by wet-chemical analysis. Moreover shown is that the valence of Ce in $(Nd_{1-x}Ce_x)_2CuO_{4+\delta}$ is not exactly +4 but ca. +3.8 as estimated on the basis of Ce $M_{4,5}$-edge XANES data.

Experimental Section

Single-phase polycrystalline samples of $(La_{1-x}Sr_x)_2CuO_{4+\delta}$ and $(Nd_{1-x}Ce_x)_2CuO_{4+\delta}$ were successfully synthesized for x ranging from 0.00 to 0.15 for the former and from 0.00 to 0.10 for the latter. The $(La_{1-x}Sr_x)_2CuO_{4+\delta}$ samples were prepared through a conventional solid-state synthesis route starting from La_2O_3, $SrCO_3$, and CuO powders thoroughly mixed into appropriate ratios. Each powder mixture was calcined at 950 °C for 12 h, then sintered in a pelletized form at 1100 °C for 20 h in an O_2 gas flow and finally annealed in the same atmosphere at 500 °C for 48 h. The $(Nd_{1-x}Ce_x)_2CuO_{4+\delta}$ samples were prepared employing a wet-chemical method in which the solution-mixed metal ions (from Nd_2O_3, $Ce(NO_3)_3 \cdot 6H_2O$, and CuO) are uniformly chelated using EDTA (ethylenediaminetetraacetic acid) as a chelating agent, as described elsewhere in detail.[3] The thus-obtained gel was burned, and the resultant raw ash was then pressed into pellets and fired in air at 1050 °C for 12 h. This yielded single-phase but not superconductive samples. To superconductorize the $(Nd_{1-x}Ce_x)_2CuO_{4+\delta}$ samples, a portion of each sample was postannealed at 1000 °C for 24 h under an oxygen partial pressure (P_{O_2}) of $\sim 3.2 \times 10^{-4}$ atm for samples with $x \leq 0.06$ and of $\sim 1.0 \times 10^{-4}$ atm for samples with $x \geq 0.065$. The level of P_{O_2} used was carefully selected for each cation composition so as to achieve the highest possible T_c value.[3]It should be noted that (as described in detail in previous studies[2,3]) such a reductive annealing is believed to eliminate the Cu vacancies existing in the as-air-synthesized $(Nd_{1-x}Ce_x)_2Cu_{1-y}O_{4+\delta}$ samples in small concentrations ($y = 0.01-0.02$) through the phase-segregation reaction: $(Nd,Ce)_2Cu_{1-y}O_{4+\delta} \rightarrow (1-y)(Nd,Ce)_2CuO_{4+\varepsilon} + y(Nd,Ce)_2O_3 + 0.5[\delta - \varepsilon + y(1+\varepsilon)]O_2$. After such annealing, the samples naturally contained minute amounts (1−2%) of the $(Nd,Ce)_2O_3$ phase. Here we however use the nominal sample composition, $y = 0$, for all the $(Nd_{1-x}Ce_x)_2CuO_{4+\delta}$ samples, i.e., both the as-air-synthesized (AS) and the reductively annealed (RA) samples.

All the samples were characterized with X-ray powder diffraction (XRD; Rigaku: RINT2000 equipped with a rotating anode; Cu K_α radiation) to confirm the expected phase composition and to determine the lattice parameters. Refinement of the lattice parameters was performed in the orthorhombic space group, *Fmmm*, for $(La_{1-x}Sr_x)_2CuO_{4+\delta}$ with $x < 0.075$ and in the tetragonal space group, *I*4/*mmm*, for $(La_{1-x}Sr_x)_2CuO_{4+\delta}$ with $x \geq 0.075$ and $(Nd_{1-x}Ce_x)_2CuO_{4+\delta}$ using the software JANA2000.[26] Superconductivity properties were measured for powdered samples under an applied magnetic field of 10 Oe using a superconducting-quantum-interference-device magnetometer (SQUID; Quantum Design: MPMS-XL). The T_c

(4) Nücker, N.; Pellegrin, E.; Schweiss, P.; Fink, J.; Molodtsov, S. L.; Simmons, C. T.; Kaindl, G.; Frentrup, W.; Erb, A.; Müller-Vogt, G. *Phys. Rev. B* **1995**, *51*, 8529. (a) Merz, M.; Nucker, N.; Schweiss, P.; Schuppler, S.; Chen, C. T.; Chakarian, V.; Freeland, J.; Idzerda, Y. U.; Klaser, M.; Muller-Vogt, G.; Wolf, Th. *Phys. Rev. Lett.* **1998**, *80*, 5192.
(5) Karppinen, M.; Yamauchi, H.; Nakane, T.; Fujinami, K.; Lehmus, K.; Nachimuthu, P.; Liu, R. S.; Chen, J. M. *J. Solid State Chem.* **2002**, *166*, 229.
(6) Merrien, N.; Coudrier, L.; Martin, C.; Maignan, A.; Studer, F.; Flank, A. M. *Phys. Rev. B* **1994**, *49*, 9906.
(7) Pham, A. Q.; Studer, F.; Merrien, N.; Maignan, A.; Michel, C.; Raveau, B. *Phys. Rev. B* **1993**, *48*, 1249.
(8) Saini, N. L.; Law, d. S-L.; Pudney, P.; Garg, K. B.; Menovsky, A. A.; Franse, J. J. M. *Phys. Rev. B* **1995**, *52*, 6219.
(9) Ghigna, P.; Spinolo, G.; Flor, G.; Morgante, N. *Phys. Rev. B* **1998**, *57*, 13426.
(10) Karppinen, M.; Kotiranta, M.; Nakane, T.; Yamauchi, H.; Chang, S. C.; Liu, R. S.; Chen, J. M. *Phys. Rev. B* **2003**, *67*, 134522. (a) Karppinen, M.; Lee, S.; Lee, J. M.; Poulsen, J.; Nomura, T.; Tajima, S.; Chen, J. M.; Liu, R. S.; Yamauchi, H. *Phys. Rev. B* **2003**, *68*, 54502.
(11) Schneider, M.; Unger, R.-S.; Mitdank, R.; Muller, R.; Krapf, A.; Rogaschewski, S.; Dwelk, H.; Janowitz, C.; Manzke, R. *Phys. Rev. B* **2005**, *72*, 14504.
(12) Pellegrin, E.; Fink, J.; Chen, C. T.; Xiong, Q.; Lin, Q. M.; Chu, C. W. *Phys. Rev. B* **1996**, *53*, 2767.
(13) Sekhar, B. R.; Studer, F.; Garg, K. B.; Moriwaki, Y.; Gasser, C.; Tanabe, K. *Phys. Rev. B* **1997**, *56*, 14809.
(14) Watanabe, T.; Kiryakov, N.; Poulsen, J.; Lee, J. M.; Chen, J. M.; Liu, R. S.; Yamauchi, H.; Karppinen, M. *Physica C* **2003**, *392–396*, 93.
(15) Karppinen, M.; Kotiranta, M.; Yamauchi, H.; Nachimuthu, P.; Liu, R. S.; Chen, J. M. *Phys. Rev. B* **2001**, *63*, 184507.
(16) Karppinen, M.; Yamauchi, H.; Morita, Y.; Kitabatake, M.; Motohashi, T.; Liu, R. S.; Lee, J. M.; Chen, J. M. *J. Solid State Chem.* **2004**, *177*, 1037.
(17) Karppinen, M.; Morita, Y.; Chen, J. M.; Liu, R. S.; Yamauchi, H. *Phys. Rev. B* **2005**, *72*, 12501. (a) Karppinen, M.; Arai, M.; Lee, J. M.; Chan, T. S.; Morita, Y.; Chen, J. M.; Liu, R. S.; Yamauchi, H. *J. Solid State Chem.* **2005**, *178*, 1705. (b) Karppinen, M.; Morita, Y.; Kobayashi, T.; Grigoraviciute, I.; Chen, J. M.; Liu, R. S.; Yamauchi, H. *J. Solid State Chem.* **2005**, *178*, 3464.
(18) Flipse, C. F. J.; Van der Laan, G.; Johnson, A. L.; Kadowaki, K. *Phys. Rev. B* **1990**, *42*, 1997.
(19) Alexander, M.; Romberg, H.; Nuecker, N.; Adelmann, P.; Fink, J.; Markert, J. T.; Maple, M. B.; Uchida, S.; Takagi, H.; Tokura, Y.; James, A. C. W. P.; Murphy, D. W. *Phys. Rev. B* **1991**, *43*, 333.
(20) Pellegrin, E.; Nuecker, N.; Fink, J.; Molodtsov, S. L.; Gutierrez, A.; Navas, E.; Strebel, O.; Hu, Z.; Domke, M.; Kaindl, G.; Uchida, S.; Nakamura, Y.; Markl, J.; Klauda, M.; Saemann-Ischenko, G.; Krol, A.; Peng, J. L.; Li, Z. Y.; Greene, R. L. *Phys. Rev. B* **1993**, *47*, 3354.
(21) Ignatov, A.; Yu, Ivanov.; A. A., Menushenkov.; A. P., Iacobucci.; S., Lagarde, P. *Phys. Rev. B* **1998**, *57*, 8671.
(22) Tranquada, J. M.; Heald, S. M.; Moodenbaugh, A. R.; Liang, G.; Croft, M. *Nature (London)* **1989**, *337*, 720.
(23) Liang, G.; Guo, Y.; Badresingh, D.; Xu, W.; Tang, Yijie.; Croft, M.; Chen, J.; Sahiner, A.; O, Beom-hoan.; Markert, J. T. *Phys. Rev. B* **1995**, *51*, 1258.
(24) Tan, Z.; Budnick, J. I.; Bouldin, C. E.; Woicik, J. C.; Cheong, S. W.; Cooper, A. S.; Espinosa, G. P.; Fisk, Z. *Phys. Rev. B* **1990**, *42*, 1037.
(25) Hsu, Y. Y.; Lin, B. N.; Ku, H. C. *J. Appl. Phys.* **2003**, *93*, 8218.
(26) Petricêk, V.; Dusek, M. *JANA2000 Crystallographic Computing System*; Institute of Physics, Academy of Sciences: Prague, Czech Republic, 2000.

value was defined at the onset temperature of the diamagnetic signal. Superconducting volume fraction was estimated from field-cooled (FC) magnetization at 5 K.

The oxygen-content parameter δ was precisely determined for each sample by means of several parallel iodometric titrations employing an analysis route carefully optimized for the present $(La_{1-x}Sr_x)_2CuO_{4+\delta}$ and $(Nd_{1-x}Ce_x)_2CuO_{4+\delta}$ samples, as described in detail elsewhere.[3] From the oxygen-content value, a value was also calculated for the valence of copper, $V(Cu)_{TTT}$, assuming the valence values of +3, +3, +2, and −2 for La, Nd, Sr, and O, respectively. The valence value of Ce was estimated at +3.82 on the basis of Ce $M_{4,5}$-edge XANES data, as to be described later in detail.

The O K-edge, Cu $L_{2,3}$-edge and Ce $M_{4,5}$-edge XANES measurements were performed on the BL20A high-energy spherical grating monochromator (HSGM) beamline of the National Synchrotron Radiation Research Center (NSRRC) in Taiwan.[15] The spectra were recorded in X-ray fluorescence-yield (I_f) mode for the O K-edge and Cu $L_{2,3}$-edge absorption, and in electron-yield (I_e) mode for the Ce $M_{4,5}$-edge absorption. The I_f data were collected utilizing a microchannel-plate (MCP) detector system with an electrically isolated grid mounted in front. The grid was set to a voltage of 50 V, the front of the MCPs to −3200 V and the rear to −200 V. The grid bias ensured that positive ions did not enter the detector, while the MCP bias ensured that no electrons were detected. The detector was located at the sample normal and photons were incident at an angle of 45° with respect to the sample normal. In the I_e mode, the sample drain current is measured. Simultaneously to I_f and I_e, the incident photon flux was monitored by a Ni mesh located after the exit slit of the monochromator. All measurements were performed on powder samples at room temperature. The photon energies were calibrated with an accuracy of 0.1 eV using the O K-edge absorption peak at 530.1 eV and the Cu L_3 white line at 931.2 eV of a CuO reference. As for the Ce $M_{4,5}$-edge spectrum the calibration was made using the absorption peak of a CeO_2 reference. The monochromator resolution was set to ∼0.22, ∼0.45, and ∼0.4 eV for the O K-edge, Cu L-edge, and Ce M-edge energy regions, respectively. The recorded spectra were corrected for the energy-dependent incident photon intensity as well as for self-absorption effects[20,27] and normalized to the tabulated standard absorption cross-sections[28] in the energy range of 600−620 eV for the O K-edge and 1000−1020 eV for the Cu L-edge.

Results and Discussion

All the $(La_{1-x}Sr_x)_2CuO_{4+\delta}$ ($0.00 \le x \le 0.15$) and $(Nd_{1-x}Ce_x)_2CuO_{4+\delta}$ ($0.00 \le x \le 0.10$) samples employed in the present study were found to be XRD-pure (except for the minute amounts of the $(Nd,Ce)_2O_3$ phase in the reductively annealed samples of the latter series). Moreover, linear variations in the lattice parameters, *a*, *b*, and *c*, with respect to the substitution level, *x*, were confirmed for both the systems: as *x* increases in $(La_{1-x}Sr_x)_2CuO_{4+\delta}$, the *a* parameter (and also the *b* parameter for the orthorhombic $x \le 0.05$ samples) decreases but the *c* parameter increases, while for $(Nd_{1-x}Ce_x)_2CuO_{4+\delta}$ just the opposite behavior is observed (see Tables 1 and 2). The lattice expansion (shrinkage) along the *c* axis is related to the larger (smaller) size of the substituent Sr^{II} (Ce^{IV}) than that of the host cation, La^{III} (Nd^{III}). On the other hand, the decreasing *a* and *b* parameters in $(La_{1-x}Sr_x)_2CuO_{4+\delta}$ and the increasing *a* parameter in $(Nd_{1-x}Ce_x)_2CuO_{4+\delta}$ directly reflect the effects of hole-doping and electron-doping, respectively, into the antibonding Cu−O orbitals in the CuO_2 plane. Moreover, for the $(Nd_{1-x}Ce_x)_2CuO_{4+\delta}$ system, the *a* parameter was confirmed to slightly increase upon the reductive annealing (Table 2), as expected.

Table 1. Characterization Results for the $(La_{1-x}Sr_x)_2CuO_{4+\delta}$ Samples: Lattice Parameters, *a*, *b*, and *c*; Values of Superconductivity Transition Temperature, T_c; Oxygen Content, $4+\delta$; and Fitted Intensities of the Peaks in the Cu L_3-Edge XANES Spectra at ∼932.6 eV [$I(Cu^{III})$]

x	*a* (Å)	*b* (Å)	*c* (Å)	T_c (K)	$4+\delta$	$I(Cu^{III})$
0.000	3.7883(1)	3.8218(1)	13.151(1)	<4	4.007(3)	0.1456
0.025	3.7841(1)	3.8048(1)	13.183(1)	<4	4.005(3)	0.3877
0.050	3.7812(1)	3.7871(1)	13.214(1)	30	4.003(3)	0.6247
0.075	3.7768(1)	3.7768(1)	13.238(1)	38	3.997(4)	0.933
0.100	3.7735(1)	3.7735(1)	13.247(1)	30	3.985(5)	1.185
0.125	3.7671(1)	3.7671(1)	13.258(1)	15	3.967(3)	1.2622
0.150	3.7655(1)	3.7655(1)	13.266(1)	<4	3.947(5)	1.3139

Cu $L_{2,3}$-Edge for $(La_{1-x}Sr_x)_2CuO_{4+\delta}$. The Cu $L_{2,3}$-edge absorption spectra recorded for the $(La_{1-x}Sr_x)_2CuO_{4+\delta}$ samples are shown in Figure 1. Here, the spectral features were normalized on the basis of the main peak in the L_3 area centered about 931.2 eV in order to clarify the appearance of spectrum for trivalent copper species. Assignment of the spectral features was straightforward on the bases of previous studies on various superconductive copper-oxide phases. For the quantitative analysis, the L_3 area (that is more intense than the L_2 area) is commonly used. The main peak in the L_3 area centered about 931.2 eV is due to formally divalent copper states, Cu^{II}, i.e., transitions from the $Cu(2p_{3/2})3d^9$ ground state to the $Cu(2p_{3/2})^{-1}3d^{10}$ excited state [$(2p_{3/2})^{-1}$ denotes a $2p_{3/2}$ hole], whereas the shoulder peak on the high-energy side of this peak about 932.6 eV is due to formally trivalent copper, Cu^{III}, i.e., transitions from the $Cu(2p_{3/2})3d^9\underline{L}$ ground state into the $Cu(2p_{3/2})^{-1}3d^{10}\underline{L}$ excited state [$\underline{L}$ denotes a ligand hole in the O 2p orbital].[4,5,20,29,30] From Figure 1, with increasing Sr content, the 931.2 eV peak becomes progressively asymmetric because of the increase in intensity of the shoulder peak for Cu^{III}. The spectral features about the Cu L_3-edge area were analyzed following refs 9–11 and 17 to gain quantitative information of the CuO_2-plane hole concentration. In brief, both the main peak (about 931.2 eV) and its shoulder (about 932.6 eV) were fitted with combined Lorentzian and Gaussian functions after approximating the background with a straight line (see the inset of Figure 1), and from the resultant integrated intensities of the peaks, i.e., $I(Cu^{II})$ and $I(Cu^{III})$, respectively, an estimate for the valence of copper was calculated as: $V(Cu)_{XAS} \equiv 2 + I(Cu^{III})/[I(Cu^{II}) + I(Cu^{III})]$. The integrated intensities of the Cu^{III} peak, $I(Cu^{III})$, are listed in Table 1. The magnitude of $I(Cu^{III})$ is clearly found to continuously increase with increasing *x*. Generally, the induced holes reside at the O site rather than at the Cu site in *p*-type doped superconductive copper oxides.[20] Therefore, the increase in $I(Cu^{III})$ is due to

(27) Tröger, L.; Arvanitis, D.; Baberschke, K.; Michaelis, H.; Grimm, U.; Zschech, E. *Phys. Rev. B* **1992**, *46*, 3283.
(28) Yeh, J. J.; Lindau, I. *At. Data Nucl. Data Tables* **1985**, *32*, 1.
(29) Nücker, N.; Fink, J.; Renker, B.; Ewert, D.; Politis, C.; Weijs, P. J. W.; Fuggle, J. C. *Z. Phys. B* **1987**, *67*, 9.
(30) Bianconi, A.; DeSantis, M.; Ciccio, A. Di.; Flank, A. M.; Fronk, A.; Fontaine, A.; Legarde, P.; Katayama-Yoshida, H.; Kotani, A.; Marcelli, A. *Phys. Rev. B* **1988**, *38*, 7196.

Table 2. Characterization Results for the As-Air-Synthesized (AS) and Reductively Annealed (RA) Samples of $(Nd_{1-x}Ce_x)_2CuO_{4+\delta}$: Lattice Parameters, a and c; Values of T_c and Superconductivity Volume Fraction; Oxygen Content, $4+\delta$; Fitted Peak Intensities of the Cu L_3-edge XANES Spectra at ~931.2 eV [$I(Cu^{II})$] and ~934 eV [$I(Cu^{I})$] and the Exact Peak Positions of the "~931.2 eV" and "~934 eV" Peaks

x	a (Å)	c (Å)	T_c (K) (vol. fraction)	$4+\delta$	$I(Cu^{II})$	$I(Cu^{I})$	Peak positions (eV)
0.000 (AS)	3.9433(1)	12.172(1)	<4	3.992(2)	5.8579	0.0482	931.20, 933.92
0.000 (RA)	3.9449(1)	12.166(1)	<4	3.982(1)	5.4422	0.0942	931.21, 933.88
0.025 (AS)	3.9448(1)	12.143(1)	<4	3.995(2)	5.4763	0.2151	931.33, 934.09
0.025 (RA)	3.9460(1)	12.139(1)	<4	3.988(2)	5.1809	0.3383	931.28, 934.07
0.050 (AS)	3.9462(1)	12.114(1)	<4	3.999(1)	5.2672	0.3915	931.33, 934.14
0.050 (RA)	3.9467(1)	12.114(1)	<4	3.994(2)	4.8902	0.4099	931.38, 934.19
0.065 (AS)	3.9470(1)	12.096(1)	<4	4.001(2)	5.0520	0.4858	931.36, 934.17
0.065 (RA)	3.9476(1)	12.096(1)	24 (3.5%)	3.997(1)	4.8169	0.5109	931.61, 934.42
0.085 (AS)	3.9481(1)	12.072(1)	<4	4.007(1)	4.7230	0.6116	931.47, 934.31
0.085 (RA)	3.9487(1)	12.072(1)	15 (16.0%)	4.003(1)	4.4877	0.6245	931.55, 934.36
0.100 (AS)	3.9491(1)	12.054(1)	<4	4.010(2)	4.4017	0.6420	931.59, 934.43
0.100 (RA)	3.9498(1)	12.056(1)	<4	4.008(2)	4.1957	0.6647	931.66, 934.50

the holes induced at the O site through Cu 3d−O 2p hybridization.[31]

Figure 2 shows the $V(Cu)_{XAS}$ values plotted for the $(La_{1-x}Sr_x)_2CuO_{4+\delta}$ system against x, together with the $V(Cu)_{TIT}$ values calculated for the same samples from the precise δ values determined by means of chemical analysis. For the entire sample series, an excellent agreement between the $V(Cu)_{XAS}$ and $V(Cu)_{TIT}$ values is revealed. Moreover, as can be seen from Figure 2, the two independent estimates for $V(Cu)$ both systematically increase with increasing x, as expected, but they also show the same trend toward saturation for the larger Sr^{II}-for-La^{III} substitution levels. This is apparently due to an increase in the oxygen-vacancy concentration with increasing x (see Table 1).

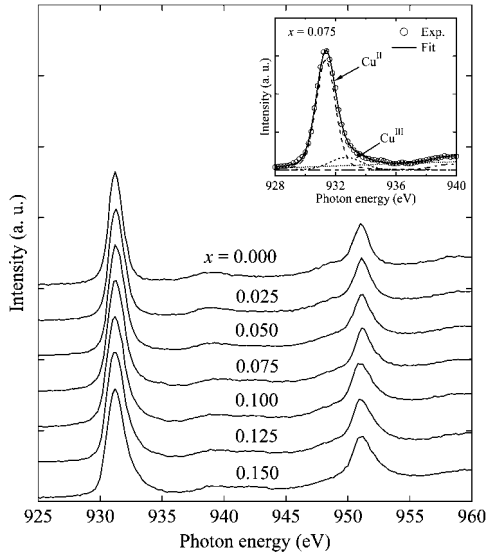

Figure 1. Cu $L_{2,3}$-edge XANES spectra for the $(La_{1-x}Sr_x)_2CuO_{4+\delta}$ samples. The inset illustrates the fitting of the spectral features about the L_3-edge into Cu^{II} and Cu^{III} components for the $x = 0.075$ sample.

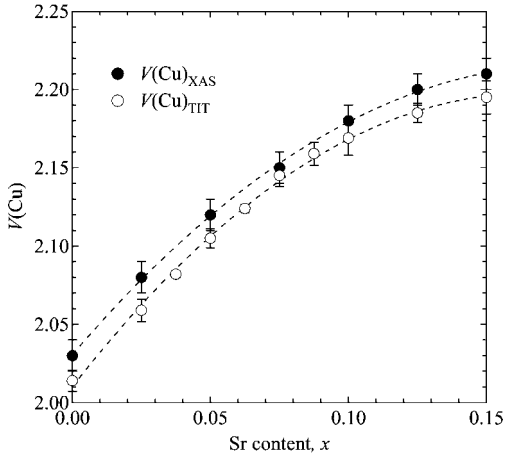

Figure 2. Valence of copper, $V(Cu)$, as estimated from the Cu L_3-edge XANES data $[V(Cu)_{XAS}]$ and the iodometric titration data $[V(Cu)_{TIT}]$ with respect to the Sr content x for the $(La_{1-x}Sr_x)_2CuO_{4+\delta}$ samples.

Ce $M_{4,5}$-Edge for $(Nd_{1-x}Ce_x)_2CuO_{4+\delta}$. In Figure 3, the Ce $M_{4,5}$-edge absorption spectra measured for representative $(Nd_{1-x}Ce_x)_2CuO_{4+\delta}$ samples are shown, together with the spectrum recorded for CeO_2 as a reference compound of tetravalent cerium. For each $(Nd_{1-x}Ce_x)_2CuO_{4+\delta}$ sample, shoulder peaks are observed on the low-energy sides of the main peaks centered around 882.5 eV (M_5-edge) and 900.1 eV (M_4-edge), in contrast to the spectrum of the CeO_2 reference, which shows only the main peaks. [Note that for unknown reasons, the low-energy shoulder peaks were not visible in the Ce $M_{4,5}$-edge XANES spectrum reported for a thin-film sample of $(Nd_{0.925}Ce_{0.075})_2CuO_{4+\delta}$.[21]] In the Ce $M_{4,5}$-edge XANES study on various Ce compounds by Kalkowski

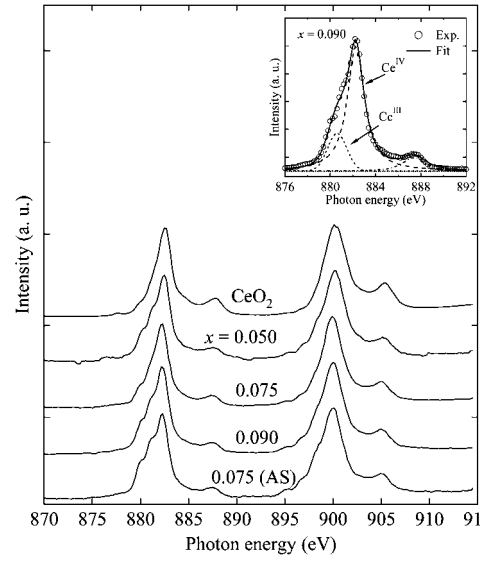

Figure 3. Ce $M_{4,5}$-edge XANES spectra for representative as-air-synthesized (AS) and reductively annealed samples of $(Nd_{1-x}Ce_x)_2CuO_{4+\delta}$. The inset illustrates the fitting of the spectral features about the M_5-edge into Ce^{III} and Ce^{IV} components for the $x = 0.090$ sample.

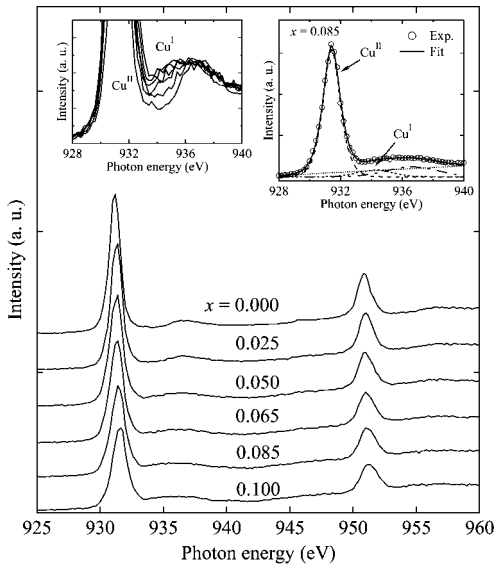

Figure 4. Cu $L_{2,3}$-edge XANES spectra for the as-air-synthesized $(Nd_{1-x}Ce_x)_2CuO_{4+\delta}$ samples. The inset illustrates the fitting of the spectral features about the L_3-edge into Cu^I and Cu^{II} components for the $x = 0.085$ sample.

et al.,[32] the low-energy shoulder peaks were interpreted as a signature of trivalent cerium. Because the shoulder peaks are clearly visible for all the present $(Nd_{1-x}Ce_x)_2CuO_{4+\delta}$ samples, we conclude that the valence of cerium, V(Ce), in $(Nd_{1-x}Ce_x)_2CuO_{4+\delta}$ is lower than +4. To gain a quantitative estimate for the V(Ce) value in $(Nd_{1-x}Ce_x)_2CuO_{4+\delta}$, we analyzed the spectral features about the M_5-edge area for the four samples displayed in Figure 3 by fitting the intensities of the main peak [$I(Ce^{IV})$] and its low-energy shoulder [$I(Ce^{III})$] and calculated the V(Ce) value as: $V(Ce) \equiv 4 - I(Ce^{III})/[I(Ce^{III}) + I(Ce^{IV})]$. For all the four $(Nd_{1-x}Ce_x)_2CuO_{4+\delta}$ samples, the V(Ce) value was determined to be $+3.82 \pm 0.05$, in good agreement with the values of +3.84 and +3.79 previously estimated on the basis of c-axis variation for polycrystalline $(Nd_{1-x}Ce_x)_2CuO_{4+\delta}$ samples[33] and thin-film samples of $(La_{1-x}Ce_x)_2CuO_{4+\delta}$,[34] respectively.

Cu $L_{2,3}$-Edge for $(Nd_{1-x}Ce_x)_2CuO_{4+\delta}$. The Cu $L_{2,3}$-edge absorption spectra obtained for the as-air-synthesized (AS) samples of $(Nd_{1-x}Ce_x)_2CuO_{4+\delta}$ are displayed in Figure 4. For the corresponding reductively annealed (RA) samples nearly identical spectra were obtained (not shown here). From Figure 4, the main peaks due to Cu^{II} (around 931.2 eV at the L_3-edge and 950.8 eV at the L_2-edge) are symmetric for all the samples, indicating nonexistence of Cu^{III} species. On the other hand, the peaks are found to systematically decrease in intensity and to gradually shift to higher energies with increasing x. These observations are consistent with those of several previous studies on the $(Nd_{1-x}Ce_x)_2CuO_{4+\delta}$ system[19–21,35] and are taken as an indication that the generated electrons are directed into the Cu site in $(Nd_{1-x}Ce_x)_2CuO_{4+\delta}$ upon the n-type doping. For the systematic shift of the peak positions with increasing x, Alexander et al.[19] have proposed three possible reasons: (i) screening effect by electrons generated upon Ce substitution, (ii) potential of Ce ions, and (iii) a change in the Madelung potential of Cu ions by the charge of Ce. From Figure 4, an additional systematic indication of the progress in electron doping appears to be the tiny but systematic enhancement of absorption intensity about 934 eV (in the L_3-edge area) with increasing x. From a single spectrum it is somewhat difficult to distinguish this peak from the weak Cu^{II} peak at ~937 eV (due to transition to the $Cu(2p_{3/2})^{-1}3d^94s$ excited state[18]), but it becomes evident once we look at the development of it with increasing x (see the left-hand side inset of Figure 4). We assign the absorption feature at ~934 eV to monovalent Cu species [i.e., transitions from the Cu $(2p_{3/2})3d^{10}$ ground state to the $Cu(2p_{3/2})^{-1}3d^{10}4s$ excited state], because the same feature is clearly observed not only for the monovalent copper-oxide compound Cu_2O[36] and oxygen-deficient samples of the $CuBa_2RCu_2O_{7-\delta}$ phase[4,5] (both containing linearly coordinated Cu^I) but also for the n-type doped samples of the so-called infinite-layer superconductor, $(Sr_{1-x}La_x)CuO_2$,[37] containing four-coordinated Cu^I. Interestingly, with increasing x, the ~934 eV peak is found to shift to higher energies with the same rate as the main peak (Table 2), such that the energy difference between the two peaks due to Cu^I and Cu^{II} remains essentially constant (~2.8 eV).

Here we use the ~934 eV peak for quantitative determination of the valence of copper in both the AS and RA samples of $(Nd_{1-x}Ce_x)_2CuO_{4+\delta}$ by analyzing the intensities of the two peaks at ~931.2 eV (due to Cu^{II}) and ~934 eV (due to Cu^I) in a way parallel to that used for the $(La_{1-x}Sr_x)_2CuO_{4+\delta}$ spectra (see the right-hand side inset of Figure 4) and calculate the valence of copper as: $V(Cu)_{XAS} \equiv 2 - I(Cu^I)/[I(Cu^I) + I(Cu^{II})]$. The individual intensity values are listed in Table 2, and the $V(Cu)_{XAS}$ values are plotted against x in Figure 5, together with the $V(Cu)_{TIT}$ values calculated for the same samples from the iodometric titration data for δ assuming $V(Ce) = +3.82$ (as revealed from the Ce $M_{4,5}$-edge XANES data). From Figure 5, it is seen that the $V(Cu)_{XAS}$ values are highly consistent with the corresponding $V(Cu)_{TIT}$ values, decreasing linearly with increasing x. Also revealed is that the decrease in $V(Cu)_{XAS}$ [and $V(Cu)_{TIT}$] upon the reductive annealing is very tiny (~0.01), particularly for the heavily Ce-substituted samples.

Superconductivity Phase Diagram for $(La_{1-x}Sr_x)_2CuO_{4+\delta}$ and $(Nd_{1-x}Ce_x)_2CuO_{4+\delta}$. The two independent experimental approaches employed here for the quantitative analysis of the valence state of copper, i.e., Cu L_3-edge XANES and iodometric titration (plus Ce M_5-edge XANES), have revealed that the influence of the reductive annealing on the V(Cu) value and accordingly on the level of carrier doping is insignificant for $(Nd_{1-x}Ce_x)_2CuO_{4+\delta}$. At the same time, such an annealing is indispensable for the appearance

(31) Mattheiss, L. F. *Phys. Rev. Lett.* **1987**, *58*, 1028.
(32) Kalkowski, G.; Kaindl, G.; Wortmann, G.; Lentz, D.; Krause, S. *Phys. Rev. B* **1988**, *37*, 1376.
(33) Huang, T. C.; Moran, E.; Nazzal, A. I.; Torrance, J. B.; Wang, P. W. *Physica C* **1989**, *159*, 625.
(34) Tsukada, A.; Naito, M.; Yamamoto, H. *Physica C* **2007**, *463–465*, 64.
(35) Fink, J.; Nuecker, N.; Romberg, H.; Alexander, M.; Nakai, S.; Scheerer, B.; Adelmann, P.; Ewert, D. *Physica C* **1989**, *162–164*, 1415.
(36) Grioni, M.; Goedkoop, J. B.; Schoorl, R.; De Groot, F. M. F.; Fuggle, J. C.; Schaefers, F.; Koch, E. E.; Rossi, G.; Esteva, J.-M.; Karnatak, R. C. *Phys. Rev. B* **1989**, *39*, 1541.
(37) Liu, R. S.; Chen, J. M.; Nachimuthu, P.; Gundakaram, R.; Jung, C. U.; Kim, J. Y.; Lee, S. I. *Solid State Commun.* **2001**, *118*, 367.

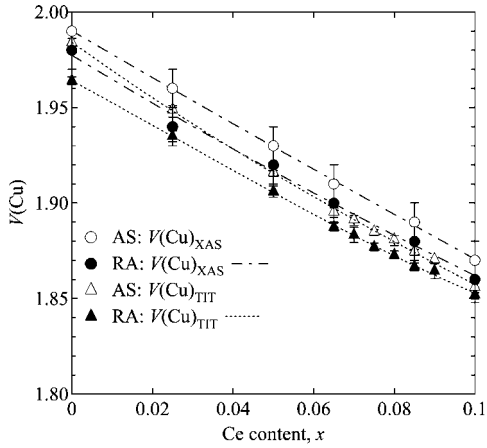

Figure 5. Valence of copper, V(Cu), as estimated from the Cu L_3-edge XANES data [$V(\mathrm{Cu})_{\mathrm{XAS}}$] and the iodometric titration data [$V(\mathrm{Cu})_{\mathrm{TIT}}$] with respect to the Ce content x, for the as-air-synthesized (AS) and reductively annealed (RA) samples of $(Nd_{1-x}Ce_x)_2CuO_{4+\delta}$.

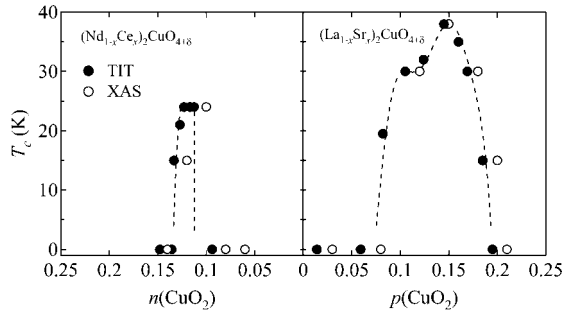

Figure 6. Relationships between the T_c value and the hole concentration $p(CuO_2)$ (right) and the electron concentration $n(CuO_2)$ (left) as estimated on the bases of the iodometric titration data (•) and the Cu L_3-edge XANES data (○) for the $(La_{1-x}Sr_x)_2CuO_{4+\delta}$ samples and the reductively annealed samples of $(Nd_{1-x}Ce_x)_2CuO_{4+\delta}$, respectively.

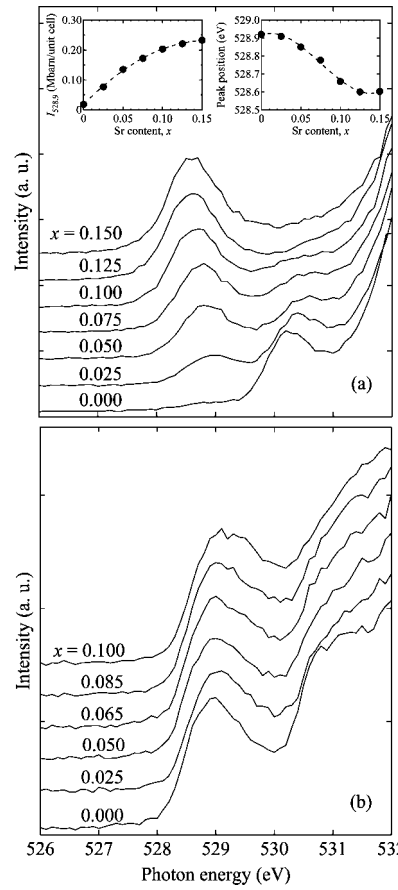

Figure 7. O K-edge XANES spectra for the (a) $(La_{1-x}Sr_x)_2CuO_{4+\delta}$ and (b) $(Nd_{1-x}Ce_x)_2CuO_{4+\delta}$ (AS) samples. The insets in the former case show the integrated intensities (left) and the exact positions (right) of the pre-edge peak about 528.9 eV with respect to the Sr content, x.

of superconductivity in the $(Nd_{1-x}Ce_x)_2CuO_{4+\delta}$ system. In fact, the appearance of superconductivity in $(Nd_{1-x}Ce_x)_2CuO_{4+\delta}$ can not be explained in terms of the V(Cu) value only: for the superconductive RA samples of $x = 0.065$ and 0.085, $V(\mathrm{Cu})_{\mathrm{XAS}}$ values of +1.90 and +1.88 [$V(\mathrm{Cu})_{\mathrm{TIT}} = +1.887$ and +1.867], respectively, were obtained, whereas for the nonsuperconductive AS sample of $x = 0.085$, $V(\mathrm{Cu})_{\mathrm{XAS}} = +1.89$ [$V(\mathrm{Cu})_{\mathrm{TIT}} = +1.875$]. Actually, the recent works on the $(Nd_{1-x}Ce_x)_2CuO_{4+\delta}$ system have quite convincingly demonstrated that rather than controlling the doping level, the low-oxygen-partial-pressure annealing repairs the Cu vacancies (which are always present in small concentrations in as-air-synthesized $(Nd_{1-x}Ce_x)_2CuO_{4+\delta}$ samples).[2,3] The present XANES results support this view.

In Figure 6, we plot the T_c values against the CuO_2-plane carrier concentration, $p(CuO_2)$ or $n(CuO_2)$, for the two prototype high-T_c superconductor systems, $(La_{1-x}Sr_x)_2CuO_{4+\delta}$ and $(Nd_{1-x}Ce_x)_2CuO_{4+\delta}$ (RA samples). The carrier concentrations were calculated as: $p(CuO_2) \equiv V(\mathrm{Cu}) - 2$ and $n(CuO_2) \equiv 2 - V(\mathrm{Cu})$, with both $V(\mathrm{Cu})_{\mathrm{XAS}}$ and $V(\mathrm{Cu})_{\mathrm{TIT}}$. From Figure 6, it is found that the highest T_c value corresponds to $p(CuO_2) \approx 0.14-0.15$ for the $(La_{1-x}Sr_x)_2CuO_{4+\delta}$ system and to $n(CuO_2) \approx 0.11-0.12$ for the $(Nd_{1-x}Ce_x)_2CuO_{4+\delta}$ system. Moreover, it is seen that the carrier-concentration range within which superconductivity appears in $(Nd_{1-x}Ce_x)_2CuO_{4+\delta}$ is much narrower than that in $(La_{1-x}Sr_x)_2CuO_{4+\delta}$. Apparently in the case of the $(Nd_{1-x}Ce_x)_2CuO_{4+\delta}$ system the concepts of "under-doping", "optimum doping", and "over-doping" do not have similar meanings as they are believed to have in the case of the p-type doped superconductive copper oxides.

O K-edge for $(La_{1-x}Sr_x)_2CuO_{4+\delta}$ and $(Nd_{1-x}Ce_x)_2CuO_{4+\delta}$. In panels a and b in Figure 7, the very pre-edge energy area (526−532 eV) of the O K-edge absorption spectra is shown for the two systems, $(La_{1-x}Sr_x)_2CuO_{4+\delta}$ and $(Nd_{1-x}Ce_x)_2CuO_{4+\delta}$ (AS samples), respectively. The spectral weight above ~531.5 eV is mainly due to the LaO/NdO planes,[19,20,29,40] and is not shown here. Also not shown are the spectra for the RA samples of $(Nd_{1-x}Ce_x)_2CuO_{4+\delta}$ that are nearly identical to those of the AS samples. For both the systems, the broad peak about 530 eV is due to transitions into O 2p states hybridized with the UHB.[4,5,12,15,35,40–43] In $(Nd_{1-x}Ce_x)_2CuO_{4+\delta}$, this feature is seen at a somewhat lower energy (~529.1 eV) than in $(La_{1-x}Sr_x)_2CuO_{4+\delta}$ (~530.2 eV).

(38) Alp, E. E.; Mini, S. M.; Ramanathan, M.; Dabrowski, B.; Richards, D. R.; Hinks, D. G. *Phys. Rev. B* **1989**, *40*, 2617.
(39) Tallon, J. L.; Bernhard, C.; Shaked, H.; Hitterman, R. L.; Jorgensen, J. D. *Phys. Rev. B* **1995**, *51*, 12911.
(40) Romberg, H.; Alexander, M.; Nuecker, N.; Adelmann, P.; Fink, J. *Phys. Rev. B* **1990**, *42*, 8768.
(41) Takahashi, T.; Katayama, H.; Matsuyama, H. *Z. Phys. B* **1990**, *78*, 343.
(42) Fink, J.; Nuecker, N.; Alexander, M.; Romberg, H.; Knupfer, M.; Merkel, M.; Adelmann, P.; Claessen, R.; Mante, G.; Buslaps, T.; Harm, S.; Manzke, R.; Skibowski, M. *Physica C* **1991**, *185–189*, 45.

Moreover, it is revealed for the $(Nd_{1-x}Ce_x)_2CuO_{4+\delta}$ system that the ~530 eV peak systematically gains intensity and gets broader with increasing Ce content, x. This is ascribed to the fact that the peak overlaps with the band due to the Ce 5d and/or Ce 4f states hybridized with O 2p states.[20,42] Here, it is important to note that for the Th-substituted analogue, $(Nd_{1-x}Th_x)_2CuO_{4+\delta}$, no change in the intensity of the peak due to UHB was observed upon increasing the doping level, x.[19] Therefore, it seems reasonable to assume that the UHB is essentially independent of the level of electron doping also in $(Nd_{1-x}Ce_x)_2CuO_{4+\delta}$. This means that the Fermi level should be located at the bottom of the UHB[24,41] and the doped electrons do not go to the O site.

On the other hand, doping the $(La_{1-x}Sr_x)_2CuO_{4+\delta}$ phase with holes results in a development of an additional pre-edge peak about 528.9 eV. Such a feature is seen in all the p-type doped copper-oxide superconductors and ascribed to the excitation of O 1s electrons to O 2p hole states in the CuO_2 plane.[4,5,12,14–17,35,40,43] For the present $(La_{1-x}Sr_x)_2CuO_{4+\delta}$ samples, we analyzed the spectral features by fitting the two pre-edge peaks at ~528.9 eV (due to CuO_2-plane hole states) and at ~530.2 eV (due to UHB) with a combination of Lorentzian and Gaussian functions after approximating the background with a quadratic line. The integrated intensity of the pre-edge peak at ~528.9 eV [$I(CuO_2)$] is displayed in the left-hand side inset of Figure 7a. With increasing x, $I(CuO_2)$ gradually increases and simultaneously the peak due to UHB decreases. The increasing $I(CuO_2)$ is in good agreement with the behavior of $V(Cu)_{XAS}$ as estimated on the bases of the Cu L_3-edge absorption spectra (Figure 2). Moreover, hole doping in $(La_{1-x}Sr_x)_2CuO_{4+\delta}$ also results in a gradual decrease in the exact position of the ~528.9 eV pre-edge peak (see the right-hand side inset of Figure 7a), reflecting the fact that the Fermi level shifts to lower energies.[44]

Conclusions

Utilizing series of high-quality samples with widely varied doping levels and independent analytical probes, i.e., O K-edge, Cu $L_{2,3}$-edge, and Ce $M_{4,5}$-edge XANES spectroscopy and wet-chemical redox analysis, we systematically studied cation valences, carrier concentrations, and electronic structures of the two prototype high-T_c superconductor systems, $(La_{1-x}Sr_x)_2CuO_{4+\delta}$ and $(Nd_{1-x}Ce_x)_2CuO_{4+\delta}$. In the hole-doped $(La_{1-x}Sr_x)_2CuO_{4+\delta}$ system, the increase in hole-doping level achieved through aliovalent Sr^{II}-for-La^{III} substitution was seen in the L_3-edge XANES spectra as the enhanced intensity of the high-energy shoulder peak at ~932.6 eV due to formally trivalent copper, whereas in the electron-doped $(Nd_{1-x}Ce_x)_2CuO_{4+\delta}$ system, the increase in electron-doping level through aliovalent Ce^{IV}-for-Nd^{III} substitution resulted in the increased intensity of the peak at ~934 eV and in the decreased intensity of the main peak at ~931.2 eV. These features of the L_3-edge spectra were utilized for quantitative analysis of the valence state of copper and accordingly of the level of carrier doping. For both the systems, the resultant values for the copper valence were highly consistent with those calculated on the basis of wet-chemical analysis. Moreover shown was that the low-oxygen-partial-pressure annealing required to superconductorize the as-air-synthesized $(Nd_{1-x}Ce_x)_2CuO_{4+\delta}$ samples does not significantly affect the Cu-valence value. From the Ce M_5-edge XANES spectra, the valence of cerium was revealed to be around +3.8 both in the as-synthesized and postannealed $(Nd_{1-x}Ce_x)_2CuO_{4+\delta}$ samples.

The present study also clearly revealed the difference between the two systems in regards to the electronic structure and superconductivity phase diagrams. The p-type doping in $(La_{1-x}Sr_x)_2CuO_{4+\delta}$ introduces holes in the valence band of predominantly O 2p character, whereas the n-type doping introduces electrons in the conduction band of predominantly Cu 3d character. In the O K-edge spectra, the increase in CuO_2-plane hole concentration with increasing x in $(La_{1-x}Sr_x)_2CuO_{4+\delta}$ was seen as the enhanced intensity of the pre-edge at ~528.9 eV, whereas for $(Nd_{1-x}Ce_x)_2CuO_{4+\delta}$ no signs were noticed that could be directly assigned to the changes in electron-doping level. Moreover, it was shown that the carrier-concentration range where superconductivity appears is much narrower in the $(Nd_{1-x}Ce_x)_2CuO_{4+\delta}$ system than the $(La_{1-x}Sr_x)_2CuO_{4+\delta}$ system. The highest T_c values were found to correspond to $n(CuO_2) \approx 0.11-0.12$ for the former and $p(CuO_2) \approx 0.14-0.15$ for the latter system.

Acknowledgment. This work was supported by Tekes (1726/31/07), Academy of Finland (114517 and 116254), and MSL's International Collaborative Research Project-2007 (Tokyo Tech).

CM800892Z

(43) Chen, C. T.; Sette, F.; Ma, Y.; Hybertsen, M. S.; Stechel, E. B.; Foulkes, W. M. C.; Schluter, M.; Cheong, S. W.; Cooper, A. S.; Rupp, L. W.; Batlogg, B.; Soo, Y. L.; Ming, Z. H.; Krol, A.; Kao, Y. H. *Phys. Rev. Lett.* **1991**, *66*, 104.

(44) Ino, A.; Mizokawa, T.; Fujimori, A.; Tamasaku, K.; Eisaki, H.; Uchida, S.; Kimura, T.; Sasagawa, T.; Kishio, K. *Phys. Rev. Lett.* **1997**, *79*, 2101.